

# Journal of Materials Chemistry A

Accepted Manuscript



This is an *Accepted Manuscript*, which has been through the Royal Society of Chemistry peer review process and has been accepted for publication.

*Accepted Manuscripts* are published online shortly after acceptance, before technical editing, formatting and proof reading. Using this free service, authors can make their results available to the community, in citable form, before we publish the edited article. We will replace this *Accepted Manuscript* with the edited and formatted *Advance Article* as soon as it is available.

You can find more information about *Accepted Manuscripts* in the [Information for Authors](#).

Please note that technical editing may introduce minor changes to the text and/or graphics, which may alter content. The journal's standard [Terms & Conditions](#) and the [Ethical guidelines](#) still apply. In no event shall the Royal Society of Chemistry be held responsible for any errors or omissions in this *Accepted Manuscript* or any consequences arising from the use of any information it contains.

# Dye-sensitized solar cells composed of photoactive composite photoelectrodes with enhanced solar energy conversion efficiency

Hong Ha Thi Vu<sup>1</sup>, Timur Sh. Atabaev<sup>1\*</sup>, Ji Young Ahn<sup>2</sup>, Nguyen Nang Dinh<sup>3</sup>, Hyung-Kook Kim<sup>1\*</sup>, Yoon-Hwae Hwang<sup>1\*</sup>

<sup>1</sup> *Department of Nano Energy Engineering, Pusan National University, Miryang 627-706, South Korea*

<sup>2</sup> *Research Center for Dielectric and Advanced Matter Physics, Pusan National University, Miryang 627-706, South Korea*

<sup>3</sup> *Department of Semiconducting Nanomaterials and Devices, University of Engineering and Technology, Hanoi National University, Hanoi, Vietnam*

Email: [atabaev@snu.ac.kr](mailto:atabaev@snu.ac.kr) (T.S. Atabaev), [hkkim@pusan.ac.kr](mailto:hkkim@pusan.ac.kr) (H.K. Kim) and [yhwang@pusan.ac.kr](mailto:yhwang@pusan.ac.kr) (Y.H. Hwang)

## Abstract

Phosphor particles were introduced as a luminescent medium to improve the overall efficiency of dye sensitized solar cells (DSSCs). In the preparation process, TiO<sub>2</sub> and the phosphor particles were mixed to make a photoelectrode with a bilayer (TiO<sub>2</sub>/mix), 3-layers (TiO<sub>2</sub>/mix/TiO<sub>2</sub>) and 4-layers (TiO<sub>2</sub>/mix/TiO<sub>2</sub>/mix) structure. The cell with the bilayered structure (TiO<sub>2</sub>/mix) after treating with a TiCl<sub>4</sub> solution showed the highest light-to-electric energy conversion efficiency (8.78%), which was ~ 25.8% higher than that of a cell with a pure TiO<sub>2</sub> layer under the same experimental conditions. The improvement in the energy conversion efficiency of the DSSCs was attributed to the phosphor enhancing incident light-harvesting via up- and down-conversion luminescence processes, resulting in an increase in the photocurrent.

## 1. Introduction

The first dye-sensitized solar cell (DSSCs) reported by Dr. Grätzel's group in 1991, is a remarkable renewable energy device with a simple method of fabrication, eco-friendly, high power conversion efficiency (PCE), and low cost [1-5]. A DSSC generally contains a

photoelectrode (PE) with a dye loaded on a nanoporous TiO<sub>2</sub> film, a platinized counter electrode and an electrolyte solution. The PE is one of the most important components for determining the PCE of cells because the absorption spectrum of the PE determines the amount of light absorbed in a cell. For DSSCs, the PCE relies to a great extent on the harvesting of incident light, and the dye plays a key role in converting that light to electrical power. Many synthetic dyes have been used to improve the light harvesting and increase the photocurrent of DSSCs. Most common Ru(II) dyes (usually N3, N719, N749), however, only absorb UV and visible light at the wavelengths between 300 and 800 nm [6], meaning that most of the solar UV and IR irradiation cannot be utilized. More incident solar light can be utilized if the UV and IR radiation can be transformed to visible light and reabsorbed by the dye molecules in the DSSCs, which will enhance the photocurrent of the DSSC.

Phosphor particles have been applied widely in many research fields, including displays [7], lasers [8], bioimaging [9], and solar cells [10, 11]. Among them, Er-doped luminescent nanomaterials are attractive from both a practical and fundamental viewpoints because of their unique optical properties arising from the intra  $4f$  transition, which gives strong visible green emission [12, 13]. Recently, some other phosphor materials have been studied as a strategy for enhancing the light conversion efficiency of DSSCs. For example, Lu<sub>2</sub>O<sub>3</sub>:Tm<sup>3+</sup>, Yb<sup>3+</sup> phosphor particles showed improved incident light harvesting via the down-conversion luminescence process and increased photocurrent. As a p-type dopant, rare-earth ions elevate the energy level of an oxide film and increase the photovoltage [14]. As a result, the PCE of DSSCs with Lu<sub>2</sub>O<sub>3</sub>:Tm<sup>3+</sup>, Yb<sup>3+</sup> doping have reached 6.63%, which is an 11.1% increase compared to the DSSCs without Lu<sub>2</sub>O<sub>3</sub>:Tm<sup>3+</sup>, Yb<sup>3+</sup> doping. Li *et al.* fabricated up-conversion hexagonal phase TiO<sub>2</sub>-NaYF<sub>4</sub>:Yb<sup>3+</sup>/Er<sup>3+</sup> microcrystals and added them to the TiO<sub>2</sub> photoanodes of DSSCs [15]. Their results suggested that TiO<sub>2</sub>-NaYF<sub>4</sub>:Yb<sup>3+</sup>/Er<sup>3+</sup> composite photoanodes can emit visible light under 495 or 980 nm excitation, and that visible light can then be absorbed by N719 dye to improve light harvesting. The PCE of the TiO<sub>2</sub>-NaYF<sub>4</sub>:Yb<sup>3+</sup>/Er<sup>3+</sup> cell was increased by 10% compared to the pure TiO<sub>2</sub> cell.

On the other hand, the PCE of DSSCs can also be improved by treating the nanoporous TiO<sub>2</sub> films with a titanium tetrachloride (TiCl<sub>4</sub>) solution followed by calcination in air, which results in the formation of TiO<sub>2</sub> crystallites on the surface of the nanoporous TiO<sub>2</sub> films [16]. The crystallites derived from the TiCl<sub>4</sub> treatment increased the surface area of the film, which

increased the absorption of dye molecules [17]. The  $\text{TiCl}_4$  treatment also reduced the charge carrier recombination; hence, it improved the PCE of the DSSCs [18, 19].

To the best of the authors' knowledge, there are no reports using a phosphor material with both DC and UC properties as a multilayer photo electrode. Therefore, the present work departs from these interesting studies in terms of the effective use of phosphor nanoparticles with DC and UC properties for enhancing the efficiency of DSSCs. A range of PE structures were created by layer-by-layer deposition, and the cell efficiency was estimated to determine the optimal fabrication conditions.

## 2. Experimental details

### 2.1. DSSC fabrication

The  $\text{TiO}_2$  pastes were prepared using the methodology described in the literature [20].  $\text{TiO}_2$  powder (P25, Sigma-Aldrich, 99.5% purity) was used with a mean particle size of approximately 21 nm. The FTO glass substrates were cleaned sequentially in acetone and ethanol with ultrasonication for 10 min each. The paste was coated on the FTO glass using the doctor blade technique, dried for 3 min at  $100^\circ\text{C}$  and the coating process was then repeated to thicken the  $\text{TiO}_2$  layer. The coated PE was then annealed at  $500^\circ\text{C}$  for 1h.

To prepare the  $\text{TiO}_2/\text{mix}$  PE,  $\text{Gd}_2\text{O}_3:1\text{mol}\% \text{Er}^{3+}$  phosphor particles were first synthesized using a previously reported procedure [21, 22]. The dried phosphor precipitates were calcined in air at  $900^\circ\text{C}$  for 2h. The  $\text{Gd}_2\text{O}_3:1\text{mol}\% \text{Er}^{3+}$  powder was dispersed further in 5 ml ethanol under ultrasonication for 20 min, and 5 ml of a  $\text{TiO}_2$  colloid solution was then added and stirred vigorously for 45 min. The  $\text{TiO}_2/\text{phosphor}$  ratio was fixed to optimum 100:6 (molar ratio) in the final solution [10, 14]. The resulting mixed colloid was deposited on the already deposited  $\text{TiO}_2$  layer via a repeated doctor blade coating and annealed at  $500^\circ\text{C}$  for 1 h. The obtained  $\text{TiO}_2/\text{mix}$  films were treated further with  $\text{TiCl}_4$  solution at  $70^\circ\text{C}$  for 0.5 h and calcined at  $500^\circ\text{C}$  for 1 h. When the sample was cooled to approximately  $90^\circ\text{C}$ , the  $\text{TiO}_2/\text{mix}$  PE was immersed in a 0.5 mM N719 (Solaronix S. A.) dye solution in ethanol at room temperature for approximately 24 h and the films were rinsed with ethanol and dried with a nitrogen stream.

The counter electrode was fabricated by dip-coating the FTO glass into a chloroplatinic acid  $\text{H}_2\text{PtCl}_6$  (Sigma-Aldrich, 37.5% Pt basis) solution followed by annealing at  $400^\circ\text{C}$  for 0.5 h. The cell was assembled by sandwiching the photo-electrode together with a counter electrode using a

100 $\mu$ m hot-melt polypropylene spacer. The space in between was filled with the liquid electrolyte (dyesol-TIMO). The other samples were also fabricated using a similar methodology to compare their conversion efficiency.

## 2.2. Characterization

The crystal phase of the prepared samples was characterized by X-ray power diffraction (XRD, Bruker D8 Discover) using Cu-K $\alpha$  ( $\lambda=0.15405$  nm) radiation. The morphology and composition of the samples was examined by scanning electron microscopy (SEM, Hitachi-S4700). Elemental analysis was carried out by energy dispersive X-ray spectroscopy (EDX; Horiba, 6853-H). The photoluminescence (PL, Hitachi F-7000) was measured using a 150W Xenon lamp as the excitation source. The UC emission spectra of the phosphor samples were recorded using a Hitachi F7000 spectrophotometer with a 975 nm diode laser as the excitation source. The current-voltage curves of the cells produced were measured under simulated AM 1.5 G illumination with a light intensity of 100 mW cm<sup>-2</sup> (Pecell Technologies Inc., PEC-L12 model) using a computer-controlled potentiostat (CHI-660B, CH Instruments). The active area of the cells was 0.16 cm<sup>2</sup>. Electrochemical impedance spectroscopy (EIS) was carried out by applying a bias of the open circuit voltage under 100 mW cm<sup>-2</sup> illumination, and the data was recorded over the frequency range, 10<sup>-1</sup> ~ 10<sup>5</sup> Hz, using a 10 mV ac signal. The Nyquist plots and Bode phase plots of the impedance data were analyzed using an equivalent circuit model and fitted with Z-view software. The incident photon to current conversion efficiencies (IPCE) were measured as a function of the wavelength from 300 to 800 nm using a solar cell spectral response measurement system (PV Measurements, Inc. QEX7).

## 3. Results and discussion

Figure 1 presents the layered photo-electrodes used for DSSC fabrication. We examined the effects of different fabrication conditions, such as a) phosphor addition and its location, and b) the TiCl<sub>4</sub> treatment effect on the overall performance of the DSSC. Both factors play an important role in enhancing the overall DSSC efficiency.

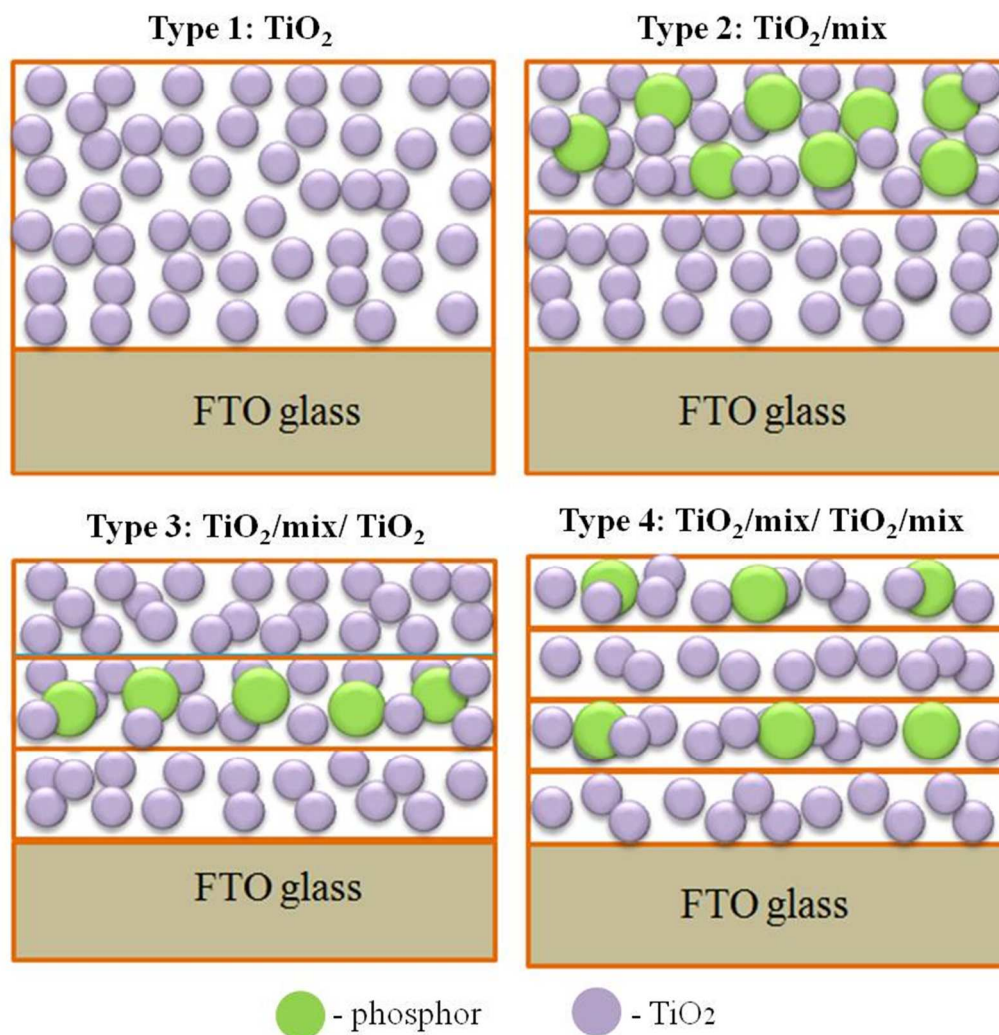


**Figure 1.** Schematic diagram of photo-electrodes for a DSSC.

Figure 2a presents a cross-sectional SEM image of a uniform 23  $\mu\text{m}$  thick doctor bladed film with  $\text{TiO}_2$  nanoparticles. The SEM images of the  $\text{Gd}_2\text{O}_3:\text{Er}^{3+}$  (Figure 2b) showed that the  $\text{Er}^{3+}$  ion doped  $\text{Gd}_2\text{O}_3$  particles consisted of monodisperse spheres with a mean particle size ranging from 180 to 250 nm. A bilayer photo-electrode was created by coating a mixing layer on top of the  $\text{TiO}_2$  nanoparticles layer (Figure 2c). The thickness of the  $\text{TiO}_2$  layer was  $\sim 12.2 \mu\text{m}$ , whereas the  $\text{TiO}_2/\text{mix}$  layer was  $\sim 11.2 \mu\text{m}$ . The phosphor particles were dispersed homogeneously within the  $\text{TiO}_2$  and a porous structure was formed throughout (Figure 2d). The phosphor particles on the surface of  $\text{TiO}_2/\text{mix}$  PE could not be observed due to the tiny phosphor particles concentration in the  $\text{TiO}_2$  colloid. EDX analysis of the  $\text{TiO}_2/\text{mix}$  surface was performed to show the presence of

phosphor particles within the  $\text{TiO}_2$ . The spectra revealed the presence of Ti, O, Gd, and Er on the surface of the  $\text{TiO}_2/\text{mix}$ , as shown in the Figure S1 (Supporting Information). Therefore,  $\text{Gd}_2\text{O}_3:\text{Er}^{3+}$  particles were confirmed to be present within the  $\text{TiO}_2$  nanoparticles.

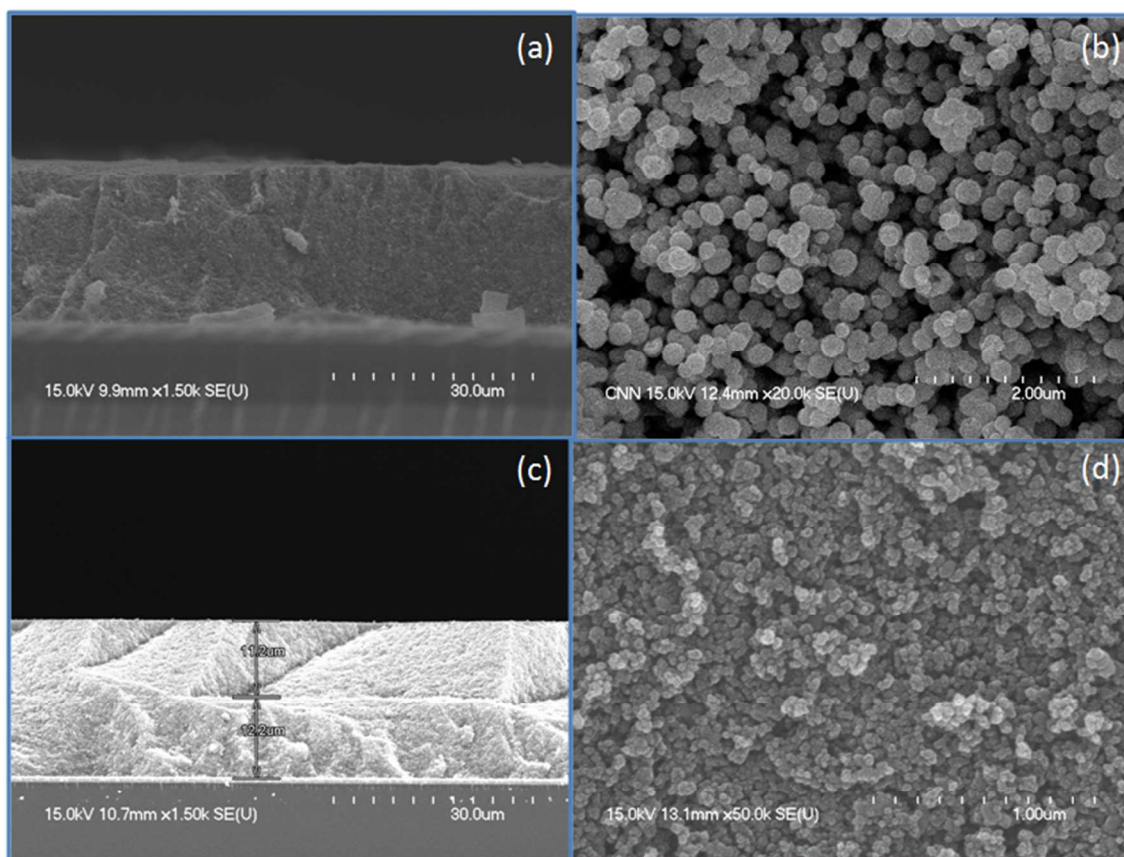


**Figure 2.** SEM images of: a) pure  $\text{TiO}_2$  film, b)  $\text{Gd}_2\text{O}_3:\text{Er}^{3+}$  phosphor particles, c)  $\text{TiO}_2$ - $\text{TiO}_2/\text{mix}$  film, and d) top-view of  $\text{TiO}_2/\text{mix}$  surface

The XRD patterns of  $\text{TiO}_2$  nanoparticles (Fig. S2, Supporting Information) showed that the nanostructures contain mixed anatase (a) and rutile (r) phases. The XRD peaks at  $25.2^\circ$ ,  $37.8^\circ$ ,  $47.9^\circ$ ,  $54.0^\circ$ , and  $55.0^\circ$   $2\theta$  were assigned to the (101), (004), (200), (105), and (211) planes of anatase  $\text{TiO}_2$  phase (JCPDS no. 21-1272), respectively. The peaks at  $27.5^\circ$ ,  $36.1^\circ$  and  $56.6^\circ$   $2\theta$  were assigned to the (110), (101) and (220) planes of the rutile phase (JCPDS no. 21-1276), respectively. Figure S3 (Supporting Information) presents the XRD pattern of  $\text{Gd}_2\text{O}_3:1\text{mol}\%$   $\text{Er}^{3+}$  particles calcined at  $900^\circ\text{C}$  for 2 h. The XRD patterns matched the characteristic peaks of

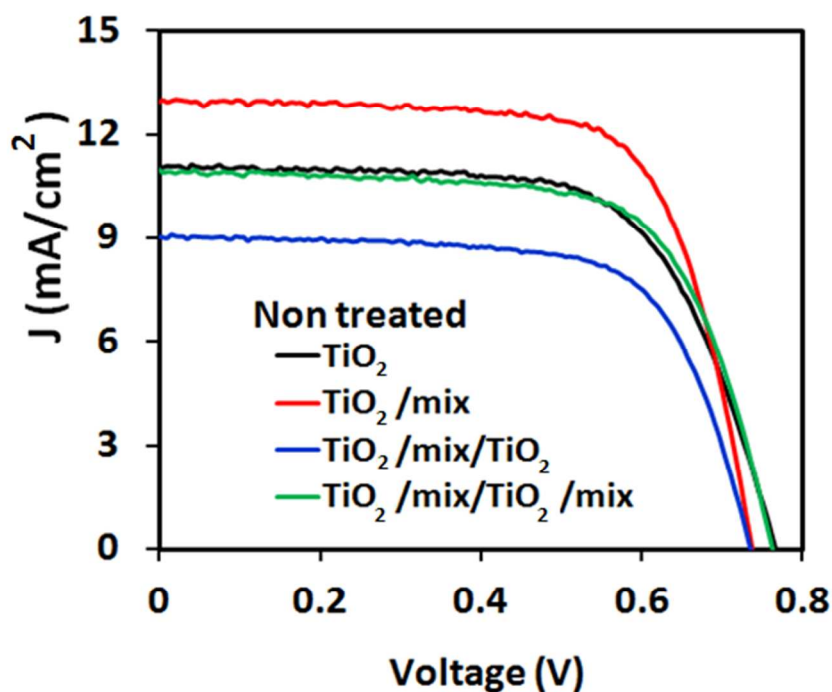
the  $\text{Gd}_2\text{O}_3$  standard cubic structure (JCPDS no. 88-2165). No additional peaks from the doped components were detected because of the low concentration of dopant ions.

Figure S4 a) (Supporting Information) shows the normalized room temperature down-conversion (DC) emission spectrum of the  $\text{Gd}_2\text{O}_3:1\%\text{Er}^{3+}$  particles under continuous 380 nm excitation. The emission peaks in the green region, at 522 nm and 537 nm, were assigned to the  ${}^2\text{H}_{11/2} \rightarrow {}^4\text{I}_{15/2}$  transition and the peaks at 550 nm and 562 nm were assigned to the  ${}^4\text{S}_{3/2} \rightarrow {}^4\text{I}_{15/2}$  transition of  $\text{Er}^{3+}$  ions. Figure S4 b) presents the up-conversion (UC) luminescence spectra of the same  $\text{Gd}_2\text{O}_3:1\% \text{Er}^{3+}$  particles with continuous 975 nm NIR excitation (Supporting Information). The optical transitions within the  $4f$  levels of  $\text{Er}^{3+}$  yield emissions bands at 482-494 nm (blue), 512-581 nm (green) and 650-675 nm (red), which were assigned to the  ${}^4\text{F}_{7/2} \rightarrow {}^4\text{I}_{15/2}$ ,  ${}^2\text{H}_{11/2}$  and  ${}^4\text{S}_{3/2} \rightarrow {}^4\text{I}_{15/2}$ , and  ${}^4\text{F}_{9/2} \rightarrow {}^4\text{I}_{15/2}$  transitions, respectively [12, 23]. According to the literature, N719 dye has the strongest absorption in the green region ( $\sim 500\text{-}550$  nm) [20]. Phosphor particles in the PEs can help to convert NIR and UV radiation into visible light photons, which can be later absorbed by N719 dye molecules. Thus, enhancement in light absorption can be achieved from the optical property of phosphor particles.

Figure 3 shows the current density-voltage characteristics of the DSSCs before the  $\text{TiCl}_4$  treatment measured with cells with an active area of  $0.16 \text{ cm}^2$  under simulated 1.5 AM solar illumination. Table 1 lists the short circuit current density ( $J_{\text{SC}}$ ), open-circuit voltage ( $V_{\text{OC}}$ ), fill factor (FF), and light to electrical energy conversion efficiency (PCE) of the DSSCs. A baseline device was fabricated with the bare  $\text{TiO}_2$  coating only on the FTO glass surface as the photo-electrode. Compared to the efficiency of the baseline device (PCE = 5.43%), the efficiency was enhanced to 6.51% using the bilayer with a  $\text{TiO}_2/\text{mix}$  photo-electrode. The current density changed with the bilayer, ranging from 11.12 to 12.98  $\text{mA}/\text{cm}^2$ . This was attributed to the improved light absorption range of N719 from the UC-DC phosphor particles in the device. On the other hand, the efficiencies of the three layered ( $\text{TiO}_2/\text{mix}/\text{TiO}_2$ ) (PCE= 4.44%) and four layered ( $\text{TiO}_2/\text{mix}/\text{TiO}_2/\text{mix}$ ) (5.41%) devices were less than that of the baseline device. This might be due to two reasons. Because  $\text{Gd}_2\text{O}_3$  is a wide band-gap material, it blocks the electron movement from the semiconductor  $\text{TiO}_2$  to the FTO glass inside the  $\text{TiO}_2$  layer. Therefore, the contact points and the interface between the  $\text{TiO}_2$  nanoparticles for the 3- and 4-layered become longer, resulting in reduced electrical contact among the nanoparticles, and reduced charge transport. In addition, the macro-pores generated by the size mismatches of  $\text{TiO}_2$  and phosphor

particles can be penetrated by the electrolyte due to the surface tension, and the charge recombination increased between the semiconductor and electrolyte. In addition, one can see that more light can be harvested (both from DC and UC processes) when mixed layer located on the top of composites (bilayer and four-layered photo-electrodes). Thus, efficiency of DSSC decreased for three layered, and then slightly increased again for four layered structure.

The improvement in the open-circuit voltage was examined by measuring the interior impedance of the cells with a different PE, which were measured by electrochemical impedance spectroscopy (EIS). The EIS spectra exhibited three typical semicircles in the Nyquist plot and three characteristic frequency peaks in the Bode phase plot in the measured frequency range, 0.1-100 kHz (Figure 4 and Figure S5, (SI)). The EIS spectra were fitted well to the corresponding equivalent circuits, as shown in Figure S6 (SI).



**Figure 3.** J-V curves of DSSCs using different PE before the treatment with  $\text{TiCl}_4$ : pure- $\text{TiO}_2$  (black),  $\text{TiO}_2/\text{mix}$  (red),  $\text{TiO}_2/\text{mix}/\text{TiO}_2$  (blue),  $\text{TiO}_2/\text{mix}/\text{TiO}_2/\text{mix}$  (green) DSSCs.

**Table 1.** Performance parameters of non-treated DSSC cells with different PEs

PE type	$J_{sc}$ (mA/cm <sup>2</sup> )	$V_{oc}$ (V)	FF(%)	PCE(%)
TiO <sub>2</sub>	11.12±0.02	0.76±0.003	63.87±0.13	5.43±0.03
TiO <sub>2</sub> /mix	12.98±0.05	0.74±0.004	68.00±0.17	6.51±0.04
TiO <sub>2</sub> /mix/ TiO <sub>2</sub>	9.02±0.06	0.73±0.005	67.09±0.25	4.44±0.13
TiO <sub>2</sub> /mix/ TiO <sub>2</sub> /mix	10.69±0.05	0.76±0.003	66.4±0.12	5.41±0.02

Table 2 lists the estimated fitted parameters. According to the literature [24], the ohmic serial resistances,  $R_s$ ,  $R_1$ ,  $R_2$ , and  $R_3$ , are associated with the series resistance of the TiO<sub>2</sub>/FTO glass substrates, interface of the electrolyte/Pt electrode, interface of the TiO<sub>2</sub>/dye/electrolyte, and electrolyte diffusion, respectively. The diameter of the first semicircle at the high frequency region presents the impedance corresponding to charge transfer at the counter electrode and/or electrical contact between the conducting substrate and TiO<sub>2</sub>. The diameter of the second semicircle at the middle frequency region provides information on the impedance at the TiO<sub>2</sub>-phosphor multilayer/dye/electrolyte interface related to charge transport/recombination, which is important for determining the efficiency of these DSSCs. The diameter of the third semicircle at the low frequency region indicates the Nernst diffusion resistance of the electrolyte. The  $R_s$ ,  $R_1$  and  $R_3$  were similar because the counter electrodes, TiO<sub>2</sub> layer coating on the FTO glass, and electrolyte were all obtained in the same way.  $R_2$ , which represents the interfacial resistance of the TiO<sub>2</sub>-dye/electrolyte interface, was 20.65  $\Omega$  for the nanoporous TiO<sub>2</sub> layer cell and 17.86  $\Omega$  for the bilayer TiO<sub>2</sub>/mix cell. In the case of the bilayer with the TiO<sub>2</sub>-phosphor mixture device, a smaller  $R_2$  indicated a decrease in the interfacial resistance, which is beneficial to the enhanced fill factor and PCE. On the other hand,  $R_2$  increases when the number of layers in the PE is increased to 3 and 4. An increase in  $R_2$  means an increase in the recombination rate and indicates low electron transfer in the cells.

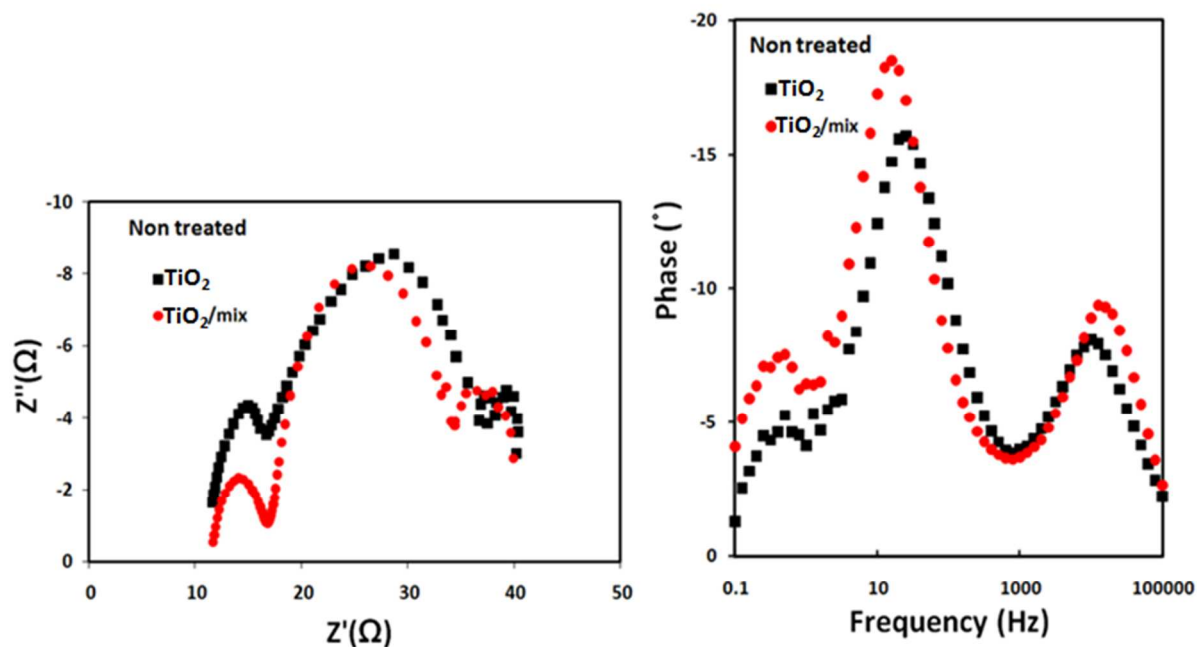


**Figure 4.** EIS Nyquist plots and Bode phase plots of the DSSCs using non treated pure- $\text{TiO}_2$  (black line) and  $\text{TiO}_2/\text{mix}$  (red line) PEs

**Table 2.** EIS parameters of DSSCs with different non-treated PEs

PE type	$R_s(\Omega)$	$R_1(\Omega)$	$R_2(\Omega)$	$R_3(\Omega)$	$\tau_e$ (ms)
$\text{TiO}_2$	11.61	4.91	20.65	4.52	7.92
$\text{TiO}_2/\text{mix}$	11.63	4.63	17.86	5.03	10.05
$\text{TiO}_2/\text{mix}/ \text{TiO}_2$	12.50	4.82	26.93	5.98	5.04
$\text{TiO}_2/\text{mix}/ \text{TiO}_2/\text{mix}$	12.13	5.18	21.01	6.02	8.08

In addition, the electron lifetime ( $\tau_e$ ) was determined from the Bode-phase plots using the following equation:

$$\tau_e = 1/2\pi f_{max}$$

where  $f_{max}$  is the maximum peak frequency in the plot. From Table 2, the longest  $\tau_e$  was observed in the case of the device with a bilayer (10.05 ms) compared to the other cases (7.92 ms for pure  $\text{TiO}_2$ , 5.04 ms for 3 layers and 8.08 ms for 4 layers). A higher  $\tau_e$  with a larger dye loading would contribute to a higher current density for the bilayer device.

Figure 5a and table 3 show the J-V characteristics of the DSSCs with different photo-electrodes after the  $\text{TiCl}_4$  treatment. The devices with the bilayer, three-layer and four-layer photoelectrodes showed a conversion efficiency of 8.78%, 8.13% and 8.21%, respectively, which is higher than that of the baseline device (PCE= 6.98%). The device with the bilayer showed the highest conversion efficiency. This increase in current density is probably due to both light scattering caused by mixing the phosphor and  $\text{TiO}_2$  layer and the good dye uptake. The optimized bilayer was used further to fabricate devices functionalized with a phosphor.

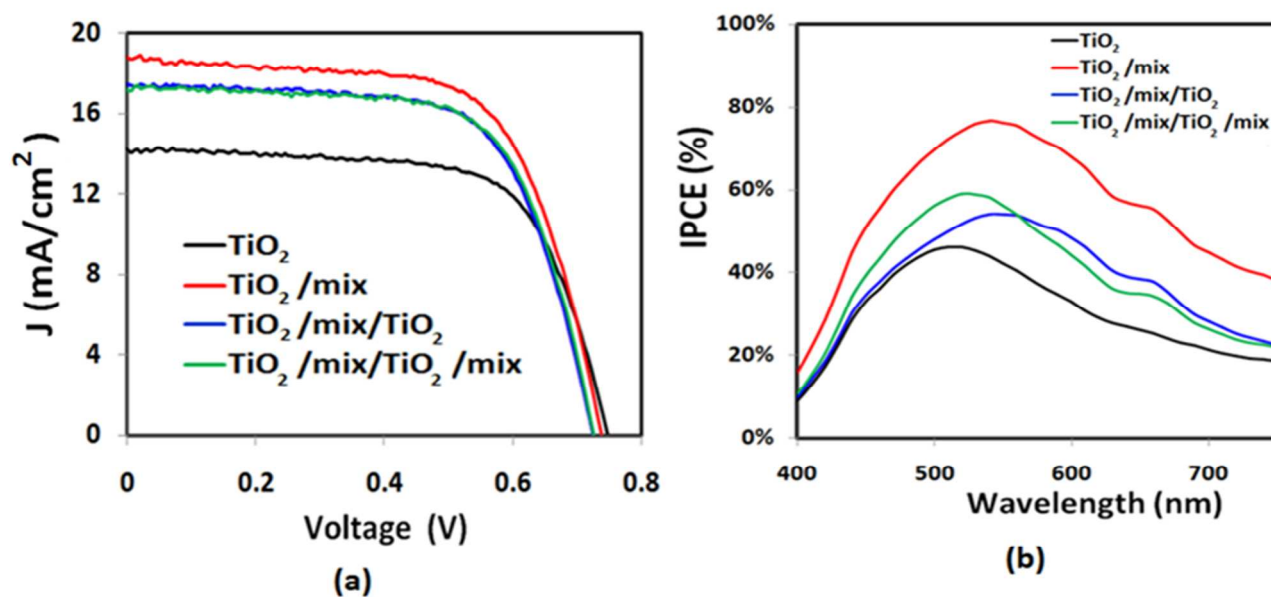


**Figure 5.** I-V curves (a) and IPCE spectra (b) of DSSCs using different PE after treat  $\text{TiCl}_4$ : pure- $\text{TiO}_2$  (black),  $\text{TiO}_2/\text{mix}$  (red),  $\text{TiO}_2/\text{mix}/\text{TiO}_2$  (blue),  $\text{TiO}_2/\text{mix}/\text{TiO}_2/\text{mix}$  (green).

As shown in Figure 5a, the current density increased for the bilayer, three layer and four layer photoelectrodes, indicating the enhanced light harvesting capability of the N719 dye molecules. Figure 5b shows the incident photo-to-current conversion efficiency spectra of the pure  $\text{TiO}_2$ , bilayer, 3-layered, and 4-layered cells. The pure  $\text{TiO}_2$  photo electrode exhibited an IPCE

maximum of 46%, whereas the devices with a bilayer, 3-layers and 4-layers showed an IPCE maximum of 77%, 54% and 59% respectively. The IPCE of the phosphor layer devices was higher in both the UV and visible regions. Also, the bilayer, 3 layer and 4 layer DSSCs showed an apparent increase in IPCE in the range from 650 to 675 nm, which was not observed in the pure TiO<sub>2</sub> PE. Compared to the pure TiO<sub>2</sub>, the bilayer, 3 layer and 4 layer devices showed higher IPCE value over a longer (>600 nm) wavelength range. This suggests that mixing of the up-/down- conversion particles make it possible for longer wavelength light to deeply penetrate the porous photo electrode layer.

Figures 6 and S7 show the EIS Nyquist plots and Bode phase plots of the cells using different treated PEs. Table 4 lists the EIS data obtained by fitting the impedance spectra of these DSSCs. The size of the second semicircle ( $R_2$ ) in the cell with pure TiO<sub>2</sub>, bilayer, 3 layers, and 4 layers was 14.84Ω, 12.63Ω, 12.81Ω, and 12.73Ω, respectively.  $R_2$  represents the interfacial resistance of the TiO<sub>2</sub>-dye/electrolyte interface and recombination of injected electron to the TiO<sub>2</sub> film with an electrolyte. The Bode phase plots displays the frequency peaks of the charge transfer process at different PE. The specific low frequency peak ( $f_{max}$ ) of the device with the bilayer, 3 layer and 4 layer electrodes shifted slightly to a lower frequency compared to the pure TiO<sub>2</sub> PE. The peak shift from a high frequency to a low frequency revealed a more rapid electron transport process. Therefore, the electron lifetime for the recombination of the cells with the bilayer, 3 layers and 4 layers are longer than the electron lifetime of the TiO<sub>2</sub> cell. These results suggest that the introduction of a TiO<sub>2</sub>-phosphor mixture as the scattering layer favors electron transfer and suppresses or reduces electron recombination.

After the TiCl<sub>4</sub> treatment, the impedance  $R_2$  decreased significantly (Figure S8 (a), SI) and the electron lifetime increased (Figure S8 (b), SI). The TiCl<sub>4</sub> treatment can enhance the connection of TiO<sub>2</sub> particles, improving charge transportation through the TiO<sub>2</sub> electrode. In summary, the lower resistance for electron transport and the longer electron lifetime for recombination could favor a higher charge collection rate of the photogenerated electrons, which enhances the efficiency of the DSSCs.

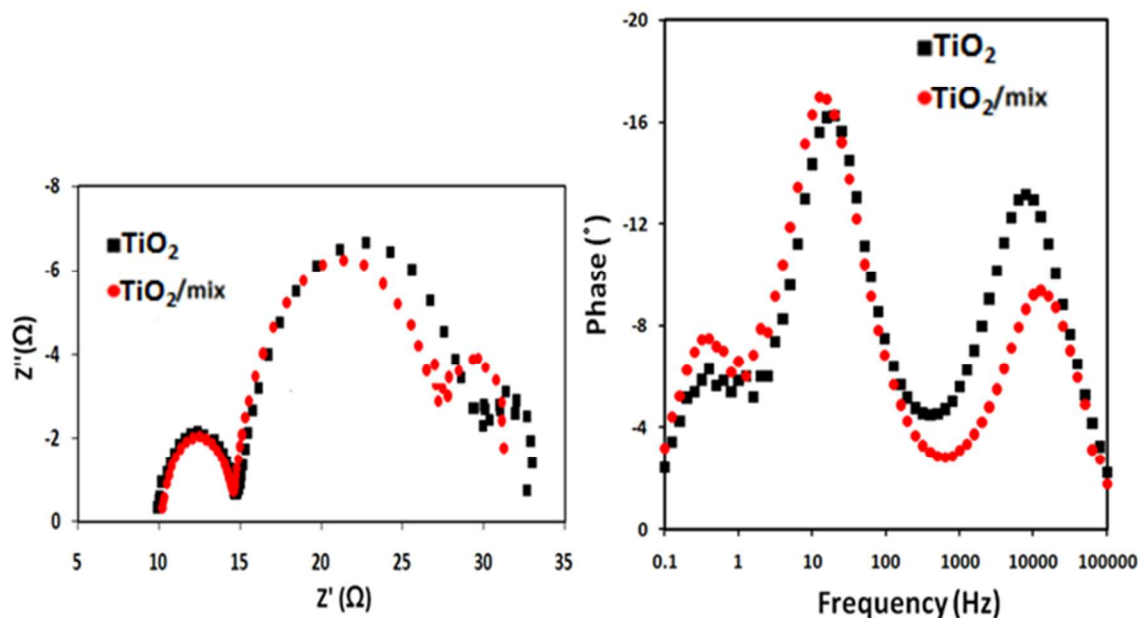


**Figure 6.** EIS Nyquist plots and Bode phase plots of the DSSCs using treated pure-TiO<sub>2</sub> (black line) and TiO<sub>2</sub>/mix (red line) PEs

**Table 3.** Performance parameters of DSSCs with different PE after treatment with TiCl<sub>4</sub> ( $\Delta PCE = (PCE - PCE_{TiO_2 PE}) / PCE_{TiO_2 PE} \times 100$ ).

PE type	$J_{sc}$ (mA/cm <sup>2</sup> )	$V_{oc}$ (V)	FF(%)	PCE(%)	$\Delta PCE$ (%)
TiO <sub>2</sub>	14.11±0.04	0.748±0.03	66.17 ±0.21	6.98±0.03	---
TiO <sub>2</sub> /mix	18.59±0.02	0.736±0.05	64.10±0.19	8.78±0.02	25.79
TiO <sub>2</sub> /mix/ TiO <sub>2</sub>	17.38±0.02	0.723±0.04	64.75±0.29	8.13±0.02	16.48
TiO <sub>2</sub> /mix/ TiO <sub>2</sub> /mix	17.26±0.03	0.725±0.07	65.65±0.37	8.22±0.05	17.76

**Table 4.** EIS parameters of DSSCs with different PE after treatment with  $\text{TiCl}_4$ .

PE type	$R_s(\Omega)$	$R_1(\Omega)$	$R_2(\Omega)$	$\tau_c$ (ms)
$\text{TiO}_2$	10.01	4.72	14.84	7.96
$\text{TiO}_2/\text{mix}$	10.21	4.38	12.63	12.65
$\text{TiO}_2/\text{mix}/ \text{TiO}_2$	10.43	4.17	12.81	10.02
$\text{TiO}_2/\text{mix}/ \text{TiO}_2/\text{mix}$	10.09	4.51	12.73	10.08

Figure S8 (c) in the Supporting Information shows the dependence of the efficiency on the different PE for the untreated and  $\text{TiCl}_4$ -treated DSSCs. The efficiencies of the devices with the  $\text{TiCl}_4$ -treated PE were higher than those of the devices without the treatment. The multilayer  $\text{TiO}_2$  and phosphor mixed with the  $\text{TiO}_2$  particles hydrolyzed from  $\text{TiCl}_4$  had the following advantages. (1) The  $\text{TiCl}_4$  treatment increases the specific surface area significantly, which favors a higher level of absorption of sensitizer dye molecules, and increases the current density in DSSCs [25, 26]. (2) The macro-pores of all the films were filled with tiny  $\text{TiO}_2$  particles from the hydrolysis of  $\text{TiCl}_4$ . The contact points and the interface between the nanoparticles become closer. Therefore, electrical contact among the nanoparticles was improved, and charge transport was enhanced.  $\text{TiO}_2$ -phosphor material mixture films with more light scattering facilitates light capture and improves the light harvesting capacity of the PE; hence, pure  $\text{TiO}_2$  has the lowest efficiency. (3) A larger number of micro-pores were produced by the tiny  $\text{TiO}_2$  particles, where the micro-pores cannot penetrate the electrolyte due to surface tension, resulting in a decrease in charge recombination between the semiconductor and electrolyte [27]. (4) The phosphor particles have up and down conversion properties. Therefore, a peak at 660 nm was observed in the IPCE spectra from UC emission at 660nm of the phosphor from the bilayer, 3 layer, 4 layer electrodes, but not in the pure  $\text{TiO}_2$  electrode. Therefore, the better efficiency parameter for the DSSC-containing phosphors than those for the DSSC lacking them indicates that the phosphor particles transfer UV light and NIR light to visible light, which the dye N719 can absorb effectively; hence, increasing the sunlight harvest and improving the efficiency of the DSSC.

#### 4. Conclusion

This paper reported an efficient method to enhance the power conversion efficiency by improving the harvesting of incident light using a TiO<sub>2</sub>-phosphor mixture on a nanoporous TiO<sub>2</sub> layer. The results showed that the additional surface treatment with TiCl<sub>4</sub> solution improves the conversion efficiency of DSSCs from 6.51% for TiO<sub>2</sub>/mix photoelectrode to 8.78%. The overall improvement in the DSSC efficiency was attributed to the improved light harvesting of dye molecules, which was achieved by the addition of phosphor particles into the photoelectrode followed by a subsequent TiCl<sub>4</sub> treatment.

#### Acknowledgement

This work was supported by the National Research Foundation of Korea (Grant no. 2012R1A1B3001357)

#### References

1. B. O'Regan, M. Grätzel, *Nature*, 1991, **353**, 737.
2. M. Grätzel, *Inorg. Chem.*, 2005, **44**, 6841.
3. M. Grätzel, *J. Photochem. Photobiol. C*, 2003, **4**, 145.
4. M. K. Nazeeruddin, P. Pechy, T. Renouard, S. M. Zakeeruddin, B. R. Humphry, P. Comte, P. Liska, L. Cevey, E. Costa, V. Shklover, L. Spiccia, G. B. Deacon, C. A. Bignozzi, M. Grätzel, *J. Am. Chem. Soc.*, 2001, **123**, 1613.
5. M. Grätzel, *Acc. Chem. Res.*, 2009, **42**, 1788.
6. M. K. Nazeeruddin, A. Kay, I. Rodicio, R. Humphry-Baer, E. Mueller, P. Liska, N. Vlachopoulos, M. Grätzel, *J. Am. Chem. Soc.*, 1993, **115**, 6382.
7. Y. P. Du, Y. W. Zhang, L. D. Sun, C. H. Yan, *J. Phys. Chem. C*, 2008, **112**, 12234.
8. L. D. Deloach, S. A. Payne, L. L. Chase, L.K. Smith, W. L. Kway, W. F. Krupke, *IEEE J. Quantum electronics*, 1993, **29**, 1179.

9. T. S. Atabaev, J. H. Lee, D. W. Han, Y. H. Hwang, H. K. Kim, *J. Biomed. Mater. Res. Part A*, 2012, **100**, 2287.
10. Q. Li, J. Lin, J. Wun, Z. Lan, Y. Wang, F. Peng, M. Huang, *J. Luminescence*, 2013, **134**, 59.
11. G. Xie, J. Wu, J. Lin, Q. Li, Z. Lan, Y. Xiao, G. Yue, H. Ye, M. Huang, *Energy Sources Part A*, 2012, **34**, 1534.
12. T. S. Atabaev, J. H. Lee, D. W. Han, H. K. Kim, Y. H. Hwang, *RSC Adv.*, 2014, **4**, 34343.
13. T. S. Atabaev, Z. Piao, Y. H. Hwang, H. K. Kim, N. H. Hong, *J. Alloys Compounds*, 2013, **572**, 113.
14. Q. Li, J. Lin, J. Wu, Z. Lan, Y. Wang, F. Peng, M. Huang, *Electrochimica Acta*, 2011, **56**, 4980.
15. Y. Li, K. Pan, G. Wang, B. Jiang, C. Tian, W. Zhou, S. Liu, F. Feng, H. Fu, *Dalton Trans.*, 2013, **42**, 7971.
16. N. Fuke, R. Katoh, A. Islam, M. Kasuya, A. Furube, A. Fukui, Y. Chiba, R. Komiya, R. Yamanaka, L. Han, H. Harima, *Energy Environ. Sci.*, 2009, **2**, 1205.
17. S. Ito, P. Liska, P. Comte, R. Charvet, P. Pechy, U. Bach, L. S. Mende, S. M. Zakeeruddin, A. Kay, M. K. Nazeeruddin, M. Grätzel, *Chem. Commun.*, 2005, 4351.
18. F. Zhao, G. Tang, J. Zhang, Y. Lin, *Electrochimica Acta*, 2012, **62**, 396.
19. J. Kim, H. Choi, C. Nahm, C. Kim, S. Nam, S. Kang, D. R. Jung, J. I. Kim, J. Kang, B. Park, *J. Power Sources*, 2012, **220**, 108.
20. W. He, T. S. Atabaev, H. K. Kim, Y. H. Hwang, *J. Phys. Chem. C*, 2013, **117**, 17894.
21. T. S. Atabaev, H. K. Kim, Y. H. Hwang, *Nanoscale Res. Lett.*, 2013, **8**, 357.
22. M. Ajmal, T.S. Atabaev, *Opt. Mater.*, 2013, **35**, 1288.
23. H. Guo, N. Dong, M. Yin, W. Zhang, L. Lou, S. Xia, *J. Phys. Chem. B*, 2004, **108**, 19205.

24. Q. Wang, J. E. Moser, M. Grätzel, *J. Phys. Chem. B*, 2005, **109**, 1494.
25. S.W. Lee, K. S. Ahn, *J. Phys. Chem.C*, 2012, **116**, 21285.
26. P. M. Sommeling, B. C. O'Regan, R. R. Haswell, H. J. P. Smit, N. J. Bakker, J. J. T. Smits, J. M. Kroon, J. A. M. van Roosmalen, *J. Phys. Chem. B*, 2006, **110**, 19191.
27. L. Liu, H. Niu, S. Zhang, L. Wan, S. Miao, J. Xu, *Applied Surface Science*, 2012, **261**, 8.